On the Production of Polyols and Hydroxycarboxylic Acids in Interstellar Analogous Ices of Methanol

Cheng Zhu, Andrew M Turner, Cornelia Meinert, Ralf I Kaiser

On the Production of Polyols and Hydroxycarboxylic Acids in Interstellar Analogous Ices of Methanol

Cheng Zhu[1,2], Andrew M. Turner[1,2], Cornelia Meinert[3*], Ralf I. Kaiser[1,2*]

[1] *Department of Chemistry, University of Hawaii at Mānoa, Honolulu, HI 96822, USA*

[2] *W.M. Keck Laboratory in Astrochemistry, University of Hawaii at Mānoa, Honolulu, HI 96822, USA*

[3]*Université Côte d'Azur, Institut de Chimie de Nice, UMR 7272 CNRS, 06108 Nice, France.*

* Corresponding author: Cornelia.Meinert@unice.fr, ralfk@hawaii.edu

Abstract

This laboratory work studied the production of complex organic molecules (COMs) in pure methanol (CH_3OH) ices exposed to ionizing radiation in the form of energetic electrons. The chemical evolution of the ices during the electron irradiation at 10 K and subsequent warm-up phase to 300 K was monitored online and in situ via Fourier Transform Infrared (FTIR) spectrometry. Polyols and hydroxycarboxylic acids related absorptions were observed in the infrared spectra of the irradiated ices and residues at room temperature. The residues were analyzed via two-dimensional gas chromatography coupled to time-of-flight mass spectrometry (GC×GC-TOFMS). Four polyols and five hydroxycarboxylic acids were detected. All of these compounds except 1,3-propanediol and 1,3-butanediol have been identified in the Murchison and Bell meteorites. The most abundant species, ethylene glycol, has also been found in the ISM. Our findings suggest that other polyols and acids may also be present in methanol-rich star-forming regions. The non-detection of higher order sugars, as those found in the ultraviolet (UV) photon processed ^{13}C-methanol ($^{13}CH_3OH$):water (H_2O):ammonia (NH_3) and ^{13}C-methanol ($^{13}CH_3OH$):water (H_2O) ice mixtures, indicates that the type of radiation source or more likely the prevalent NH_3 and/or H_2O molecules in the ISM are critical to the abiotic formation of the bio-essential sugars. Experiments are currently being designed to elucidate the roles of each component.

1. Introduction

Over the last few decades, polyols – organic compounds containing multiple hydroxyl (-OH) groups – and hydroxycarboxylic acids – carboxylic acids (RCOOH) carrying one or more additional hydroxyl groups – have received substantial attention from the astronomy and laboratory astrochemistry communities due to their potential importance for astrobiology (Agarwal et al. 1985; Cooper et al. 2001; Hollis et al. 2002; Bennett et al. 2007; Nuevo et al. 2010; Maity et al. 2014; Nuevo & Sandford 2014; Kaiser et al. 2015; Maity et al. 2015; Meinert et al. 2016; Bergantini et al. 2017; Bergantini et al. 2018; Modica et al. 2018; Zhu et al. 2019). Ethylene glycol ($HOCH_2CH_2OH$), the simplest polyol, represents the only polyol detected in the gaseous interstellar medium (ISM) toward, e.g., Sagittarius B2(N-LMH) (Hollis, et al. 2002) and the MM1 core in the high-mass star-forming region NGC 6334I (McGuire et al. 2017) (Table 1). However, a rich spectrum of polyols and hydroxycarboxylic acids has been detected in the Murchison and Bell meteorites (Table 1) (Cooper, et al. 2001; Monroe & Pizzarello 2011; Cooper & Rios 2016). The presence of biologically related molecules, such as glycerol ($HOCH_2CH(OH)CH_2OH$) as a central precursor to lipids, and glyceric acid ($HOCH_2CH(OH)COOH$) being crucial in glycolysis in primitive meteorites, is consistent with the scenario that a significant amount of the organic compounds related to the biological processes on the early Earth might have been delivered by extraterrestrial objects to Earth (Oró 1961; Chyba & Sagan 1992).

In addition to searching for extraterrestrial sources, laboratory experiments exploiting ultraviolet (UV) light and energetic particles exposing interstellar analogous ice mixtures at low temperatures (10 to 80 K) have been performed in an attempt to simulate the formation of polyols and hydroxycarboxylic acids under astrophysical, non-biological conditions (Table 1). Nevertheless, very often, these simulation experiments have been affected by contaminants. (Agarwal, et al. 1985) irradiated ice mixtures of carbon monoxide (CO) - ammonia (NH_3) - water (H_2O) with broad UV light at 10 K and tentatively identified ethylene glycol and glycerol in the residues. However, the authors admitted that these polyols are likely contaminants in the methanol used to extract the residues. In order to distinguish photochemical products from contaminants, irradiation experiments using isotopically labelled ices (^{13}CO: $^{15}NH_3$:$H_2{}^{18}O$) were conducted; these studies detected ethylene glycol ($HOCH_2CH_2OH$), glycerol ($HOCH_2CH(OH)CH_2OH$), glycolic acid ($HOCH_2COOH$), lactic acid ($CH_3CH(OH)COOH$), and

3-hydroxypropionic acid ($HOCH_2CH_2COOH$) (Table 1) (Briggs et al. 1992). Nonetheless, the experimental intensities of the labeled and unlabeled species are highly inconsistent with expected isotopic patterns making the results tentative. (Materese et al. 2014) analyzed UV-irradiated nitrogen (N_2):^{13}C-methane ($^{13}CH_4$):^{13}CO ices, but were only able to identify five acids (Table 1). Recent studies introduced methanol (CH_3OH) to ice mixtures (Nuevo, et al. 2010; Meinert, et al. 2016; Nuevo et al. 2018) as methanol is ubiquitous in the ISM at levels up to 30% of water in interstellar ices (Boogert et al. 2008; Bottinelli et al. 2010). (Meinert, et al. 2016) detected the most extensive polyols thus far, hydroxycarboxylic acids, and even ribose ($HCO(CHOH)_4H$) in the residues of photo processed H_2O:$^{13}CH_3OH$:NH_3 ices. Since these studies used mixtures of $^{13}CH_3OH$ with H_2O or H_2O and NH_3, it is challenging to reveal the role of each precursor in the reactions. Formose-type reactions, which do not involve ammonia, were proposed as the formation pathways of aldehyde and sugars (Shigemasa et al. 1977; Meinert, et al. 2016), however, aldehydes – glycolaldehyde ($HOCH_2CHO$), lactaldehyde ($CH_3CH(OH)CHO$), and glyceraldehyde ($HOCH_2CH(OH)CHO$) – were not detected in the residues of photo processed H_2O:$^{13}CH_3OH$ ices, but present in the experiments with addition of ammonia (de Marcellus et al. 2015). These findings indicate that ammonia may participate in the formation of even nitrogen-free aldehydes and sugars and complicate the understanding of the detailed reaction mechanisms. Furthermore, the sources of oxygen (from $^{13}CH_3OH$ or H_2O) in the detected products are unknown as well. Therefore, it is essential to perform experiments exploiting pure methanol first to examine its role in the formation of these complex organic molecules. Previous simulation experiments using pure methanol ices (Chen et al. 2013; Henderson & Gudipati 2015; Kaiser, et al. 2015; Maity, et al. 2015; Sullivan et al. 2016) confirmed simple polyols and hydroxycarboxylic acids, such as ethylene glycol ($HOCH_2CH_2OH$), glycerol ($HOCH_2CH(OH)CH_2OH$), and glycolic acid ($HOCH_2COOH$), during the temperature programmed desorption (TPD) phase of UV-light or energetic electrons processed ices.

Here, to rule out any contamination and to simplify the complexity of untangling possible reaction routes, we performed experiments of exposing pure CH_3OH as well as $CH_3{}^{18}OH$ ices to energetic electrons simulating cascades of secondary electrons generated by galactic cosmic rays (GCRs) penetrating interstellar ices (Kaiser et al. 1997; Kaiser & Roessler 1997; Bennett et al. 2005) and analyzed the solid residues generated in the warm-up phase of the irradiated ices from

10 K to 300 K. By using ^{18}O substituted methanol, we reveal that ethylene glycol ($HOCH_2CH_2OH$), 1,3-propanediol ($HOCH_2CH_2CH_2OH$), glycolic acid ($HOCH_2COOH$), 3-hydroxypropionic acid ($HOCH_2CH_2COOH$), 3-hydroxybutyric acid ($CH_3CH(OH)CH_2COOH$), 4-hydroxybutyric acid ($HOCH_2CH_2CH_2COOH$), glycerol ($HOCH_2CH(OH)CH_2OH$), and glyceric acid ($HOCH_2CH(OH)COOH$) can be generated from the electron-irradiation of pure methanol. Furthermore, we detected a new species 1,3-butanediol ($HOCH_2CH_2CH(OH)CH_3$), which has not been identified in previous laboratory residues. Methanol has been found to be ubiquitous in interstellar ices such as Orion BN and AFGL989 at levels of up to 30% with respect to water (Gibb et al. 2004). Since no laboratory simulation experiment can reproduce the chemical complexity and diverse radiation conditions of actual interstellar space simultaneously, we performed experiments using simple pure methanol ices first (Chen, et al. 2013; Henderson & Gudipati 2015; Kaiser, et al. 2015; Maity, et al. 2015; Sullivan, et al. 2016) before extending to more complex systems. Our experiments were conducted at doses of 168.9 ± 26.1 eV per methanol molecule representing typical life times of long-lived interstellar molecular clouds at ages of about 50 million years (Yeghikyan 2011; Jeffreson & Kruijssen 2018). No higher order sugars were found in the extractions of the residues, indicating that at least at doses below 168.9 ± 26.1 eV molecule^{-1} water and/or ammonia may be critical for the formation of biologically relevant sugars detected in the residues of UV photon-processed H_2O:$^{13}CH_3OH$:NH_3 and H_2O:$^{13}CH_3OH$ ices (de Marcellus, et al. 2015; Meinert, et al. 2016; Nuevo, et al. 2018).

2. Experimental methods

The experiments were carried out in a contamination-free ultrahigh vacuum (UHV) chamber operating at a base pressure of 9×10^{-11} Torr (Zheng et al. 2006; Kaiser et al. 2013), which was achieved using two magnetically suspended turbo molecular pumps (Osaka TG420 MCAB) coupled to two oil-free scroll pumps (Anest Iwata ISP-500). Within the chamber, a highly polished silver wafer was attached to an oxygen free high conductivity (OFHC) copper target and cooled by a two-stage closed cycle helium cryostat (CTI-Cryogenics 9600). After the wafer reached 10.0 ± 0.3 K, degassed methanol (CH_3OH; Sigma-Aldrich, 99.9%) or ^{18}O-methanol ($CH_3{}^{18}OH$; Sigma-Aldrich, 95 atom % ^{18}O) was deposited on the substrate using a precision leak valve and glass capillary array at a pressure of 2×10^{-7} Torr in the main chamber for approximately 15 min. The ice growth was monitored in situ via laser interferometry with a

helium-neon (He-Ne) laser (CVI Melles Griot; 25-LHP-230, 632.8 nm) (Turner et al. 2015). The laser beam struck the silver wafer at an angle of 2° relative to the ice surface normal and was reflected to a photodiode (CVI Melles Griot Silicon Photodiode; CVI Xll-632.8-12.6M) interfaced to a picoammeter (Keithley 6485). Considering the refractive index of methanol ice (n_{CH_3OH} = 1.33 ± 0.04) (Bouilloud et al. 2015), the ice thickness was calculated to be 900 ± 50 nm. The infrared spectra of the ices were recorded in a range of 6,000 to 400 cm^{-1} with 4 cm^{-1} spectral resolution using a Nicolet 6700 Fourier Transform Infrared (FTIR) spectrometer (Figure 1 (a)). With the absorption coefficients of 1.01 × 10^{-16} and 1.40 × 10^{-18} cm $molecule^{-1}$ for the 3270 cm^{-1} (ν_1) and 1120 cm^{-1} (ν_{11}) bands (Bouilloud, et al. 2015), respectively, the column density of methanol was found to be (1.5 ± 0.2) × 10^{18} molecules cm^{-2}. Taking into account the density of methanol (ρ_{CH_3OH} = 1.01 ± 0.03 g cm^{-3}) (Bouilloud, et al. 2015), the ice thickness was calculated to be 800 ± 100 nm, which agrees well with the value determined using the laser interferometry method (900 ± 50 nm).

The ices were then irradiated isothermally at 10.0 ± 0.3 K with 5 keV electrons (Specs EQ 22-35 electron source) at a 15° angle relative to the target surface (3.2 ± 0.3 cm^2) for 1 hour at nominal current of 5000 nA with an extraction efficiency of the electrons of 78 %. Exploiting Monte Carlo simulations (Casino 2.42) (Drouin et al. 2007), the average and maximum penetration depths of the electrons were found to be 420 ± 40 nm and 675 ± 70 nm (Table 2), respectively, which is less than the ice thickness of 900 ± 50 nm ensuring no interaction between the electrons and the silver wafer. The average dose was calculated to be 168.9 ± 26.1 eV per methanol molecule. The irradiated ices were kept at 10.0 ± 0.3 K for one hour and then annealed at a rate of 1 K min^{-1} to 300 K (temperature-programmed desorption, TPD). During the irradiation and TPD phases, in situ FTIR spectra were recorded in intervals of 2 minutes (Figure 1, Tables 3-5).

After each experiment, the residue on the wafer was analyzed by a two-dimensional gas chromatographic (GC×GC) Pegasus IV D instrument coupled to a time-of-flight mass spectrometer ((TOFMS), LECO, St. Joseph, Michigan, USA) (Figure 2, Table 6). The TOFMS system operated at a storage rate of 150 Hz, with a 25–700 amu mass range, a detector voltage of 1.6 kV, and a solvent delay of 10 min. The ion source and transfer temperatures were set to 503 K. The column set consisted of an Agilent J&W DB 5MS Ultra Inert primary column (30 m ×

0.25 mm inner diameter (ID), 0.25 μm film thickness) Press-Tight (Restek, Bellefonte, USA) connected to an Agilent DB Wax secondary column (1.40 m × 0.1 mm ID, 0.1 μm film thickness). Helium was used as carrier gas at a constant flow rate of 1 mL min^{-1}. Sample volumes of 1 μL were injected in the splitless mode into an ultra-inert, single taper splitless inlet liner with glass wool (Agilent) at an injector temperature of 503 K. All samples were analyzed with the identical temperature program. The primary oven was operated as follows: 313 K for 1 min, temperature increase of 5 K min^{-1} to 463 K and held for 9 min. The secondary oven used the same temperature program with a constant temperature offset of 288 K except for the glycerol standard where a constant temperature offset of 303 K was used. The latter explains the faster elution time of glycerol in the second dimension of the glycerol standard (R_{t2} = 1.28 s) compared to glycerol detected in all other injected samples (R_{t2} = 1.40 s, Table 6). A modulation period of 5 s was applied for the liquid nitrogen cooled thermal modulator. Data were acquired and processed with LECO Corp ChromaTOF software. Compound identification was performed by comparison with the chromatographic retention in both dimensions and mass spectra of authentic standards.

The derivatization reagents including *N*,*O*-bis(trimethylsilyl)trifluoroacetamide (BSTFA), trimethylsilyl chloride (TMCS), the internal standard methyl laurate, and hexane as well as the reference standards of the polyols (ethylene glycol and glycerol), the saccarinic acid (glyceric acid), and the hydroxycarboxylic acids (glycolic, 3-hydroxypropionic, S-3-hydroxybutyric, and 4-hydroxybutyric) were purchased from Sigma Aldrich. Sample-handling glassware was wrapped in aluminum foil and heated at 773 K for 3 h prior to usage to eliminate possible contamination. Eppendorf tips were sterile and the water used for extraction, standard solutions, reagent solutions, and blanks was of high-performance liquid chromatography grade. The residues were extracted with 6 × 50 μL water from their silver wafers and transferred into conical reaction vials (1 mL V-Vial, Wheaton). The aqueous extracts were dried under a gentle stream of nitrogen and silylated with an excess of 35 μL BSTFA and 5 μL TMCS for 2 h at 353 K in the presence of the internal standard methyl laurate in hexane (5 μL, 10^{-5} M). The derivatized mixtures were transferred into GC vials for their subsequent GC×GC−TOFMS analysis. Procedural blanks were run in sequence to each sample in order to monitor significant background interferences. To eliminate any ^{16}O contaminants, residues of the ^{18}O-methanol ($CH_3{}^{18}OH$) experiments were analyzed.

3. Results & Discussion

3.1 FTIR

Figure 1(b) depicts the FTIR spectra of the irradiated CH_3OH and $CH_3{}^{18}OH$ ices at 10.0 K. Table 4 compiles the assignments of the irradiation induced peaks. In addition to the decomposition of the precursor and formation of carbon dioxide (CO_2), carbon monoxide (CO), methane (CH_4), formaldehyde (H_2CO), and formyl radicals (HCO) (Bennett, et al. 2007; Maity, et al. 2015), essential absorptions in the ranges of 1000−1100 cm^{-1} ($\nu_{(C-O)}$), 1750−1700 cm^{-1} ($\nu_{(C=O)}$), and 3600−3000 cm^{-1} ($\nu_{(O-H)}$) were identified, which are related to functional groups of hydroxycarboxylic acids and/or polyols (Socrates 2004). These features are obscured by the precursor CH_3OH but remain in the residue at 300 K (Figure 1(c), Table 5). Experiments with $CH_3{}^{18}OH$ match the isotopic red shifts for the $\nu_{(C-O)}$ and $\nu_{(C=O)}$ modes by 20−30 cm^{-1} (Friedel et al. 1967; Maity, et al. 2015). These findings suggest that *functional groups* linked to hydroxycarboxylic acids and polyols can be generated by exposure of pure methanol ice to ionization radiation; however, functional groups are not unique to specific molecules due to the overlapping of the absorptions of homologous series and/or isomers (Socrates 2004). Therefore, the infrared analysis does not identify individual hydroxycarboxylic acid or polyol molecules.

3.2 GC×GC−TOFMS

To identify discrete molecular species, the residues were extracted, silylated, and analyzed via GC×GC−TOFMS (Figure 2 and Table 6). Compound identification was performed by comparison with the chromatographic retention in both dimensions of authentic standards and their corresponding mass spectra, as well as with previously reported data on trimethylsilyl (TMS) derivatives of polyols and hydroxycarboxylic acids (Meinert, et al. 2016). Table 6 summarizes the retention times of analytes in the first and second chromatographic dimension as well as the corresponding mass spectra of the analyzed residue and standard. Figure 3 depicts the structures of the identified compounds in the residue. Four polyols and five hydroxycarboxylic acids were identified with an elution sequence of ethylene glycol, 1,3-propanediol, glycolic acid, 1,3-butanediol, 3-hydroxypropionic acid, 3-hydroxybutyric acid, 4-hydroxybutyric acid, glycerol, and glyceric acid. All of the following discussions about mass spectra are based on ^{18}O substituted species. The mass spectra of all identified compounds are characterized by the intrinsic mass fragments of trimethyl silylated derivatives, i.e. by the absent molecular ion $[M]^+$

peak, the fragment ion $[M–15]^+$ formed by the loss of a methyl group from the $(CH_3)_3Si$-protecting group as well as silicon-containing fragments at *m*/*z* = 45 [CH_3SiH_2], 73 [$(CH_3)_3Si$], 75 [$(CH_3)_3SiH_2$], and 149 [$(CH_3)_5Si_2{}^{18}O$]. Favored α-cleavage with charge retention followed by loss of trimethylsilanol group [$((CH_3)_3)Si–{}^{18}OH$] (*m*/*z* = 92) is observed as the predominant fragmentation pathway for all hydroxycarboxylic acids as well as polyols (McLafferty 1959; Gross 2004). Moreover, all hydroxycarboxylic acids undergo a McLafferty-type rearrangement (ester migration) of a $(CH_3)_3Si$ group (McLafferty 1959; Gross 2004) (Table 6). Glycerol and glyceric acid exhibit a common mass fragment of *m*/*z* = 209 $[(CH_3)_3Si{}^{18}OCH{=}CH_2{}^{18}OSi(CH_3)_3]^+$, which is indicative of a vicinal diol group. Glyceric acid has a characteristic fragmentation pattern of stepwise loss of a methyl group (CH_3), a trimethylsilanol group [$((CH_3)_3)Si–{}^{18}OH$], and carbon monoxide ($C{}^{18}O$) inducing the fragment of *m*/*z* = 193 $[(CH_3)_2Si{}^{18}OCH{=}CH{}^{18}OSi(CH_3)_3]^+$ ($[M–15–92–30]^+$) (Meinert, et al. 2016).

3.3. Reaction pathways

Having explicitly identified fully ^{18}O substituted polyols and hydroxycarboxylic acids in the residues of irradiated and ^{18}O-methanol ($CH_3{}^{18}OH$) ices, we are now proposing possible formation pathways (Scheme 1). Sophisticated infrared studies coupled with kinetics studies on the formation of small reaction intermediates and products reveal that upon exposure to energetic electrons at 10 K, methanol (CH_3OH) can decompose via atomic hydrogen loss leading to the methoxy (CH_3O) (reaction (1)) and hydroxymethyl radical (CH_2OH) (reaction (2)); likewise, retro-insertion of electronically excited oxygen atoms ($O(^1D)$) forms methane (CH_4) (reaction (3)) (Bennett, et al. 2007; Maity, et al. 2014). Further, fragmentation of the methoxy (CH_3O) and hydroxymethyl radical (CH_2OH) yields formaldehyde (H_2CO) (reactions (4) and (5)), which then is eventually radiolyzed to carbon monoxide (CO) in one step through elimination of molecular hydrogen (reaction (6)) or via two steps involving the formyl (HCO) radical (reaction (7) and (8)) (Bennett, et al. 2007). Then, atomic oxygen formed in reaction (3) may react with carbon monoxide generated via reaction (6) to yield carbon dioxide (CO_2) (reaction (9)) (Bennett et al. 2004; Bennett et al. 2009a, 2009b). Therefore, the initial decomposition and radiolysis forms primary (CH_3O, CH_2OH, CH_4) and higher order products, e.g. carbon dioxide (CO_2) (Bennett, et al. 2007).

The hydroxymethyl radical (CH_2OH) has been shown to recombine with a second hydroxymethyl radical (CH_2OH) barrierlessly leading to the formation of ethylene glycol (reaction (10)) (Scheme 1) (Butscher et al. 2015; Zhu, et al. 2019). Likewise, the hydroxycarbonyl radical (HOCO) – generated via reaction of suprathermal hydrogen atoms with carbon dioxide (reaction (11)) – can react with carbon-centered radicals also barrierlessly (Bennett & Kaiser 2007; Kim & Kaiser 2010; Zhu et al. 2018); here, the hydroxycarbonyl radical (HOCO) may react with the hydroxymethyl radical (CH_2OH) to yield glycolic acid (reaction (12)). Further, the hydroxymethyl radical (CH_2OH) can recombine also without barrier with a methyl radical (CH_3) generated via hydrogen loss from methane (reaction (13)) (Bennett et al. 2006; He et al. 2010; Jones & Kaiser 2013; Abplanalp et al. 2018) to ethanol (CH_3CH_2OH) (reaction (14)) (Bergantini, et al. 2018). Note that ethanol was not detected in room temperature residues since this molecule sublimes quantitatively between 130 K and 150 K as the irradiated ice is warmed up to 300 K (Bergantini, et al. 2017; Bergantini, et al. 2018). These products (ethylene glycol, glycolic acid, ethanol) represent critical building blocks in the molecular mass growth to higher order polyols and hydroxycarboxylic acids.

Radiolysis of ethylene glycol, glycolic acid, and ethanol followed by reactions with key primary (CH_2OH, CH_4) and higher order (CO_2) species can synthesize three-carbon-containing species: glycerol, glyceric acid, 3-hydroxypropionic acid, 1-propanol, and 1,3-propanediol (reactions (15) to (22)). In detail, radiolysis of ethylene glycol via hydrogen atom loss forms the 1,2-dihydroxyethyl radical ($HOCH_2CHOH$) (reaction (15)) which then recombines with a hydroxymethyl radical (CH_2OH) to glycerol (reaction (16)) (Kaiser, et al. 2015; Fedoseev et al. 2017). The methyl-carboxyhydroxy radical (HOCHCOOH) (Leroy et al. 1991) – generated via decomposition of glycolic acid (reaction (17)) – can react with a hydroxymethyl radical (CH_2OH) forming glyceric acid (reaction (18)). Radiolysis of ethanol produces 2-hydroxyethyl radical (CH_2CH_2OH) (reaction (19)), which can recombine with hydroxycarbonyl (HOCO), methyl (CH_3), and hydroxymethyl (CH_2OH) radicals generating 3-hydroxypropionic acid (reaction (20)), 1-propanol (reaction (21)), and 1,3-propanediol (reaction (22)), respectively.

Four-carbon-containing species can be generated in similar radical-radical recombination reactions. In detail, electron irradiation of 3-hydroxypropionic acid, 1-propanol, and 1,3-propanediol can generate ethyl-2-carboxy-1-hydroxy ($HOCHCH_2COOH$) (reaction (23)), 3-hydroxypropyl ($CH_2CH_2CH_2OH$) (Ferro-Costas et al. 2018) (reaction (24)), and propyl-1,3-

dihydroxy ($HOCH_2CH_2CHOH$) (Buley et al. 1966) (reaction (25)) radicals, which then recombine with methyl (CH_3), hydroxycarbonyl (HOCO), and methyl (CH_3) radicals producing 3-hydroxybutyric acid (reaction (26)), 4-hydroxybutyric acid (reaction (27)), and 1,3-butanediol (reaction (28)), respectively.

Quantification of the detected molecules supports the proposed 'bottom up' reaction pathways involving stepwise mass growth processes. As shown in Table 6, the sequences of the relative amount of each species with respect to ethylene glycol are found to be ethylene glycol (100.00%) > glycerol ((14.67 ± 1.47)%), glycolic acid ((19.58 ± 1.93)%) > glyceric acid ((1.85 ± 0.18)%), 3-hydroxypropionic acid ((13.41 ± 1.34)%) > 3-hydroxybutyric acid ((4.83 ± 0.48)%), and 1,3-propanediol ((9.86 ± 0.99)%) > 1,3-butanediol ((5.21 ± 0.52)%). These results are consistent with the proposal that glycerol, glyceric acid, 3-hydroxybutyric acid, and 1,3-butanediol are secondary products of ethylene glycol, glycolic acid, 3-hydroxypropionic acid, and 1,3-propanediol, respectively (Scheme 1). Previous analysis of the volatile organic compounds released during a warming-up phase of a photoprocessed methanol ice also found that the abundances of C2 to C4 compounds decrease with the increase of their carbon chain length (Abou Mrad et al. 2016). Note that since the identified products were generated in solid-phase, numerous primary and secondary reactions might be coupled. Deciphering all possible elementary reactions is infeasible and out of the scope of this study. The identified molecules may also be generated in the TPD phase.

4. Astrophysical Implications

In the present study, we observe the formation of four polyols, ethylene glycol ($HOCH_2CH_2OH$), 1,3-propanediol ($HOCH_2CH_2CH_2OH$), glycerol ($HOCH_2CH(OH)CH_2OH$), and 1,3-butanediol ($HOCH_2CH_2CH(OH)CH_3$) – and five hydroxycarboxylic acids – glycolic acid ($HOCH_2COOH$), glyceric acid ($HOCH_2CH(OH)COOH$), 3-hydroxypropionic acid ($HOCH_2CH_2COOH$), 3-hydroxybutyric acid ($CH_3CH(OH)CH_2COOH$), and 4-hydroxybutyric acid ($HOCH_2CH_2CH_2COOH$) – in methanol ices upon interaction with ionizing radiation at 10 K, at radiation doses equivalent to those interstellar ices received during the lifetime of long-lived molecular clouds of about few 10^7 years. These molecules were detected in the extractions of the room-temperature residues of the irradiated ^{18}O-methanol ($CH_3{}^{18}OH$) ice using GC×GC−TOFMS. Since our derivatization reagents do not react with aldehydes (no –OH group),

these species, such as formaldehyde (H_2CO), acetaldehyde (CH_3CHO), glyoxal (OCHCHO), and methylglyoxal (CH_3COCHO), were not detected in the residues. All detected polyols and hydroxycarboxylic acids except 1,3-propanediol and 1,3-butanediol have been identified in the Murchison and Bell meteorites (Cooper, et al. 2001; Monroe & Pizzarello 2011; Cooper & Rios 2016). Among these compounds, the most abundant one, ethylene glycol, has been detected in methanol-rich comets, such as C/1995 O1 (Hale-Bopp) (Crovisier et al. 2004) and 67P/Churyumov–Gerasimenko (Altwegg et al. 2017; Schuhmann et al. 2019). The double focusing mass spectrometer (DFMS) of the Rosetta Orbiter Spectrometer for Ion and Neutral Analysis (ROSINA) instrument suite onboard the Rosetta Spacecraft detected signals at m/z = 92, which could be linked to glycerol (Altwegg, et al. 2017). However, major fragments of glycerol are missing indicating that the peak at m/z = 92 may be mainly contributed by toluene (C_7H_8) (Schuhmann, et al. 2019). Ethylene glycol has also been found in the ISM (Hollis, et al. 2002; McGuire, et al. 2017). Our findings suggest that methanol-rich star-forming regions are probably good candidates for future astronomical searches for these molecules, especially the central backbone of lipids – glycerol – since its formation efficiency is second only to ethylene glycol.

Note that no higher order sugars were detected in our residues. However, previous studies found extensive sugars from C_3 to C_5, including the essential component of ribonucleic acid (RNA) and adenosine triphosphate (ATP) – ribose ($HCO(CHOH)_4H$), in the residues of UV-light irradiated $^{13}CH_3OH$:NH_3:H_2O ice mixtures (Meinert, et al. 2016). Exposure of $^{13}CH_3OH$:H_2O ices to UV-radiation generated the sugar of DNA, 2-deoxyribose (Nuevo, et al. 2018). The differences between the present work and previous studies are radiation sources (energetic electrons vs UV photons), energy doses, and ice compositions ($CH_3{}^{18}OH$ vs $^{13}CH_3OH$:NH_3:H_2O and $^{13}CH_3OH$: H_2O). Previous studies have investigated the effects of each precursor on products properties (Bernstein et al. 1995; Muñoz Caro & Schutte 2003; Nuevo et al. 2011; Henderson & Gudipati 2015; Abou Mrad et al. 2017; Fresneau et al. 2017). Methanol was found to be the most reactive species and the main source of oxygen in products (Bernstein, et al. 1995; Henderson & Gudipati 2015; Fresneau, et al. 2017). The fraction of ammonia in the precursors does not alter the O/C ratio of the products significantly (Fresneau, et al. 2017). An excess of H_2O can increase the abundance of more complex molecules due to molecular trapping effects (Fresneau, et al. 2017), which may explain why high order sugars are missing in this study as our precursor is only pure methanol. We do not rule out the possibility of more complex

sugars in our residues but out of detection limit since the generation efficiency decreases upon increasing of molecular complexity (Abou Mrad, et al. 2016) and our analytical protocol did not specifically target sugar molecules. Future experiments by exposing $CH_3{}^{18}OH$:H_2O and $CH_3{}^{18}OH$:NH_3:H_2O ice mixtures to energetic electrons are planned to investigate if the type of radiation source or the prevalent NH_3 and H_2O molecules in the ISM (Mottl et al. 2007), or both, play critical roles in the abiotic formation of bio-essential sugars.

Acknowledgements

The Hawaii group acknowledges support from the US National Science Foundation, Division of Astronomical Sciences under grant AST-1800975. C. M. received funding by the French government through the UCAJEDI Investments in the Future Project managed by the National Research Agency (ANR) with the reference number ANR-15-IDEX-01 and the European Research Council under the European Union's Horizon 2020 research and innovation program (grant agreement 804144).

References

Abou Mrad, N., Duvernay, F., Chiavassa, T., & Danger, G. 2016, MNRAS, 458, 1234

Abou Mrad, N., Duvernay, F., Isnard, R., Chiavassa, T., & Danger, G. 2017, ApJ, 846, 124

Abplanalp, M. J., Jones, B. M., & Kaiser, R. I. 2018, PCCP, 20, 5435

Agarwal, V., Schutte, W., Greenberg, J., et al. 1985, OLEB, 16, 21

Altwegg, K., Balsiger, H., Berthelier, J.-J., et al. 2017, MNRAS, 469, S130

Bennett, C. J., Chen, S.-H., Sun, B.-J., Chang, A. H., & Kaiser, R. I. 2007, ApJ, 660, 1588

Bennett, C. J., Jamieson, C., Mebel, A. M., & Kaiser, R. I. 2004, PCCP, 6, 735

Bennett, C. J., Jamieson, C. S., & Kaiser, R. I. 2009a, ApJS, 182, 1

Bennett, C. J., Jamieson, C. S., & Kaiser, R. I. 2009b, PCCP, 11, 4210

Bennett, C. J., Jamieson, C. S., Osamura, Y., & Kaiser, R. I. 2006, ApJ, 653, 792

Bennett, C. J., & Kaiser, R. I. 2007, ApJ, 660, 1289

Bennett, C. J., Osamura, Y., Lebar, M. D., & Kaiser, R. I. 2005, ApJ, 634, 698

Bergantini, A., Góbi, S., Abplanalp, M. J., & Kaiser, R. I. 2018, ApJ, 852, 70

Bergantini, A., Maksyutenko, P., & Kaiser, R. I. 2017, ApJ, 841, 96
Bernstein, M. P., Sandford, S. A., Allamandola, L. J., Chang, S., & Scharberg, M. A. 1995,
Boogert, A. C., Pontoppidan, K. M., Knez, C., et al. 2008, ApJ, 678, 985
Bottinelli, S., Boogert, A. A., Bouwman, J., et al. 2010, ApJ, 718, 1100
Bouilloud, M., Fray, N., Benilan, Y., et al. 2015, MNRAS, 451, 2145
Briggs, R., Ertem, G., Ferris, J., et al. 1992, OLEB, 22, 287
Buley, A., Norman, R., & Pritchett, R. 1966, JCSBPO, 849
Butscher, T., Duvernay, F., Theule, P., et al. 2015, MNRAS, 453, 1587
Chen, Y.-J., Ciaravella, A., Caro, G. M., et al. 2013, ApJ, 778, 162
Chyba, C., & Sagan, C. 1992, Natur, 355, 125
Cooper, G., Kimmich, N., Belisle, W., et al. 2001, Natur, 414, 879
Cooper, G., & Rios, A. C. 2016, PNAS, 113, E3322
Crovisier, J., Bockelée-Morvan, D., Biver, N., et al. 2004, A&A, 418, L35
de Marcellus, P., Meinert, C., Myrgorodska, I., et al. 2015, PNAS, 112, 965
Drouin, D., Couture, A. R., Joly, D., et al. 2007, Scanning, 29, 92
Fedoseev, G., Chuang, K.-J., Ioppolo, S., et al. 2017, ApJ, 842, 52
Ferro-Costas, D., Martínez-Núñez, E., Rodríguez-Otero, J., et al. 2018, JPCA, 122, 4790
Fresneau, A., Abou Mrad, N., d'Hendecourt, L. L., et al. 2017, ApJ, 837, 168
Friedel, R., Durie, R., & Shewchyk, Y. 1967, Carbon, 5, 559
Gibb, E. L., Whittet, D. C. B., Boogert, A. C. A., & Tielens, A. G. G. M. 2004, ApJS, 151, 35
Gross, J. H. 2004, Mass Spectrometry-A Textbook (1st ed.; Heidelberg: Springer)
He, J., Gao, K., Vidali, G., Bennett, C. J., & Kaiser, R. I. 2010, ApJ, 721, 1656
Henderson, B. L., & Gudipati, M. S. 2015, ApJ, 800, 66
Hollis, J. M., Lovas, F. J., Jewell, P. R., & Coudert, L. 2002, ApL, 571, L59
Jeffreson, S. M., & Kruijssen, J. D. 2018, MNRAS, 476, 3688
Jones, B. M., & Kaiser, R. I. 2013, JPCL, 4, 1965
Kaiser, R., Eich, G., Gabrysch, A., & Roessler, K. 1997, ApJ, 484, 487
Kaiser, R., & Roessler, K. 1997, ApJ, 475, 144
Kaiser, R., Stockton, A., Kim, Y., Jensen, E., & Mathies, R. 2013, ApJ, 765, 111
Kaiser, R. I., Maity, S., & Jones, B. M. 2015, AChIE, 54, 195
Kim, Y., & Kaiser, R. I. 2010, ApJ, 725, 1002

Leroy, G., Sana, M., & Wilante, C. 1991, JMoStT, 228, 37

Maity, S., Kaiser, R. I., & Jones, B. M. 2014, FaDi, 168, 485

Maity, S., Kaiser, R. I., & Jones, B. M. 2015, PCCP, 17, 3081

Materese, C. K., Cruikshank, D. P., Sandford, S. A., et al. 2014, ApJ, 788, 111

McGuire, B. A., Shingledecker, C. N., Willis, E. R., et al. 2017, ApL, 851, L46

McLafferty, F. W. 1959, AnaCh, 31, 82

Meinert, C., Myrgorodska, I., De Marcellus, P., et al. 2016, Sci, 352, 208

Modica, P., Martins, Z., Meinert, C., Zanda, B., & d'Hendecourt, L. 2018, ApJ, 865, 41

Monroe, A. A., & Pizzarello, S. 2011, GeCoA, 75, 7585

Mottl, M. J., Glazer, B. T., Kaiser, R. I., & Meech, K. J. 2007, ChGC, 67, 253

Muñoz Caro, G. M., & Schutte, W. A. 2003, A&A, 412, 121

Nuevo, M., Bredehöft, J. H., Meierhenrich, U. J., d'Hendecourt, L., & Thiemann, W. H.-P. 2010, AsBio, 10, 245

Nuevo, M., Cooper, G., & Sandford, S. A. 2018, NatCo, 9, 5276

Nuevo, M., Milam, S. N., Sandford, S. A., et al. 2011, AdSpR, 48, 1126

Nuevo, M., & Sandford, S. A. 2014, ApJ, 793, 125

Oró, J. 1961, Natur, 190, 389

Schuhmann, M., Altwegg, K., Balsiger, H., et al. 2019, ESC, 3, 1854

Shigemasa, Y., Matsuda, Y., Sakazawa, C., & Matsuura, T. 1977, BChSJ, 50, 222

Socrates, G. 2004, Infrared and Raman Characteristic Group Frequencies (3rd ed.; New York: John Wiley & Sons, Ltd.)

Sullivan, K. K., Boamah, M. D., Shulenberger, K. E., et al. 2016, MNRAS, 460, 664

Turner, A. M., Abplanalp, M. J., Chen, S. Y., et al. 2015, PCCP, 17, 27281

Yeghikyan, A. 2011, Ap, 54, 87

Zheng, W., Jewitt, D., & Kaiser, R. I. 2006, ApJ, 648, 753

Zhu, C., Frigge, R., Bergantini, A., Fortenberry, R. C., & Kaiser, R. I. 2019, ApJ, 881, 156

Zhu, C., Turner, A. M., Abplanalp, M. J., & Kaiser, R. I. 2018, ApJS, 234, 15

Figures

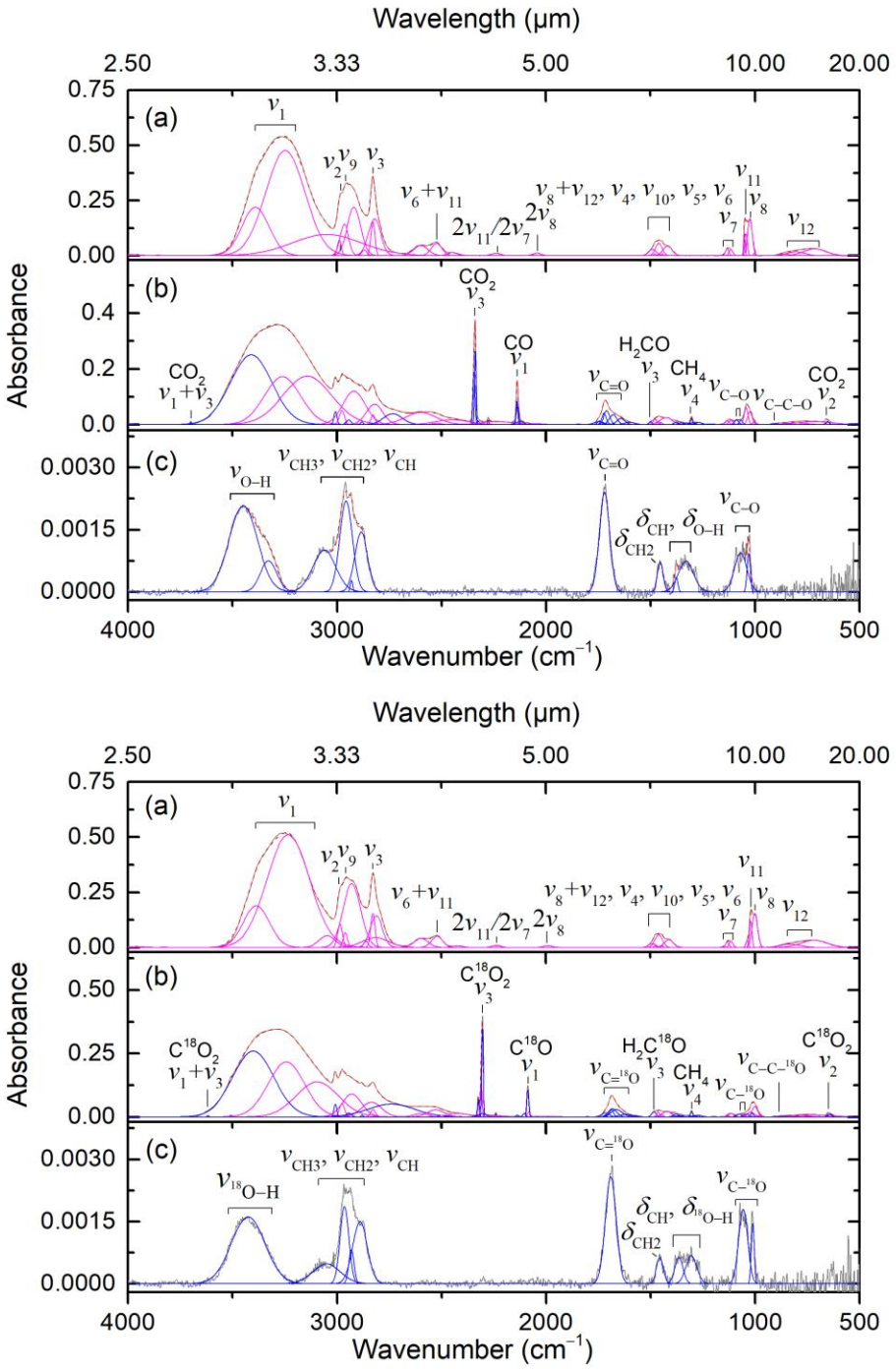

Figure 1. Deconvoluted infrared spectra of CH_3OH (top) and $CH_3{}^{18}OH$ (bottom) ices: (a) before the irradiation, (b) after the irradiation at 10 K, and (c) the residue at 300 K. Blue peaks represent absorptions induced by the irradiation. For clarity, only significant peaks are labeled; detailed assignments are compiled in Tables 3-5.

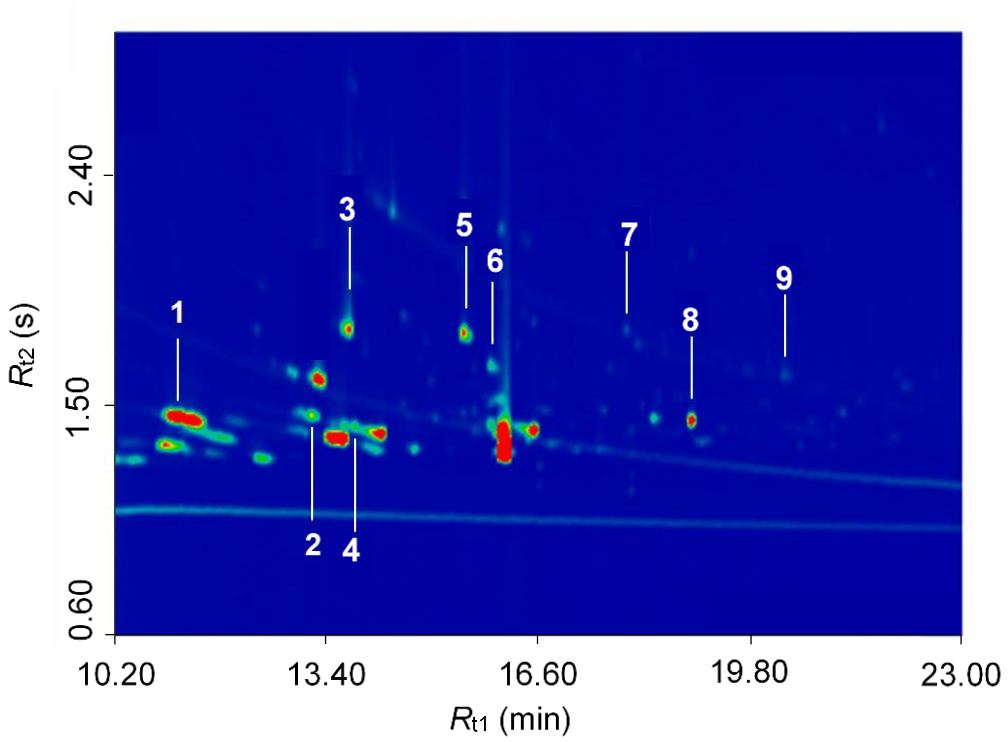

Figure 2. GC×GC-TOFMS chromatogram of the solvated residues of the irradiated $CH_3{}^{18}OH$ ices. Identified compounds include: (1) ethylene glycol, (2) 1,3-propanediol, (3) glycolic acid, (4) 1,3-butanediol, (5) 3-hydroxypropionic acid, (6) 3-hydroxybutyric acid, (7) 4-hydroxybutyric acid, (8) glycerol, and (9) glyceric acid.

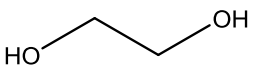

Ethylene glycol

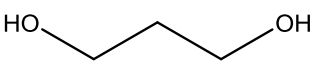

1,3-Propanediol

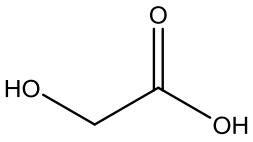

Glycolic acid

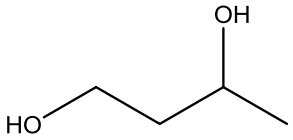

1,3-Butanediol

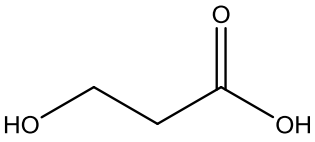

3-Hydroxypropionic acid

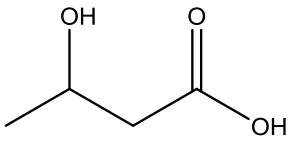

3-Hydroxybutyric acid

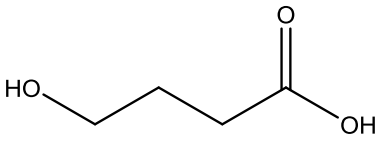

4-Hydroxybutyric acid

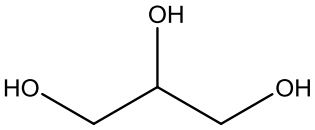

Glycerol

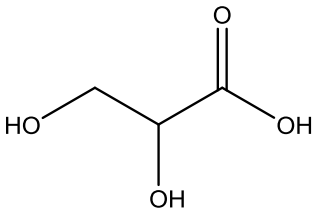

Glyceric acid

Figure 3. Molecular structures of ^{18}O labeled compounds in irradiated $CH_3{}^{18}OH$ ices by GC×GC-TOFMS. 1,3-Butanediol-^{18}O is a new species which has not been reported in previous laboratory studies.

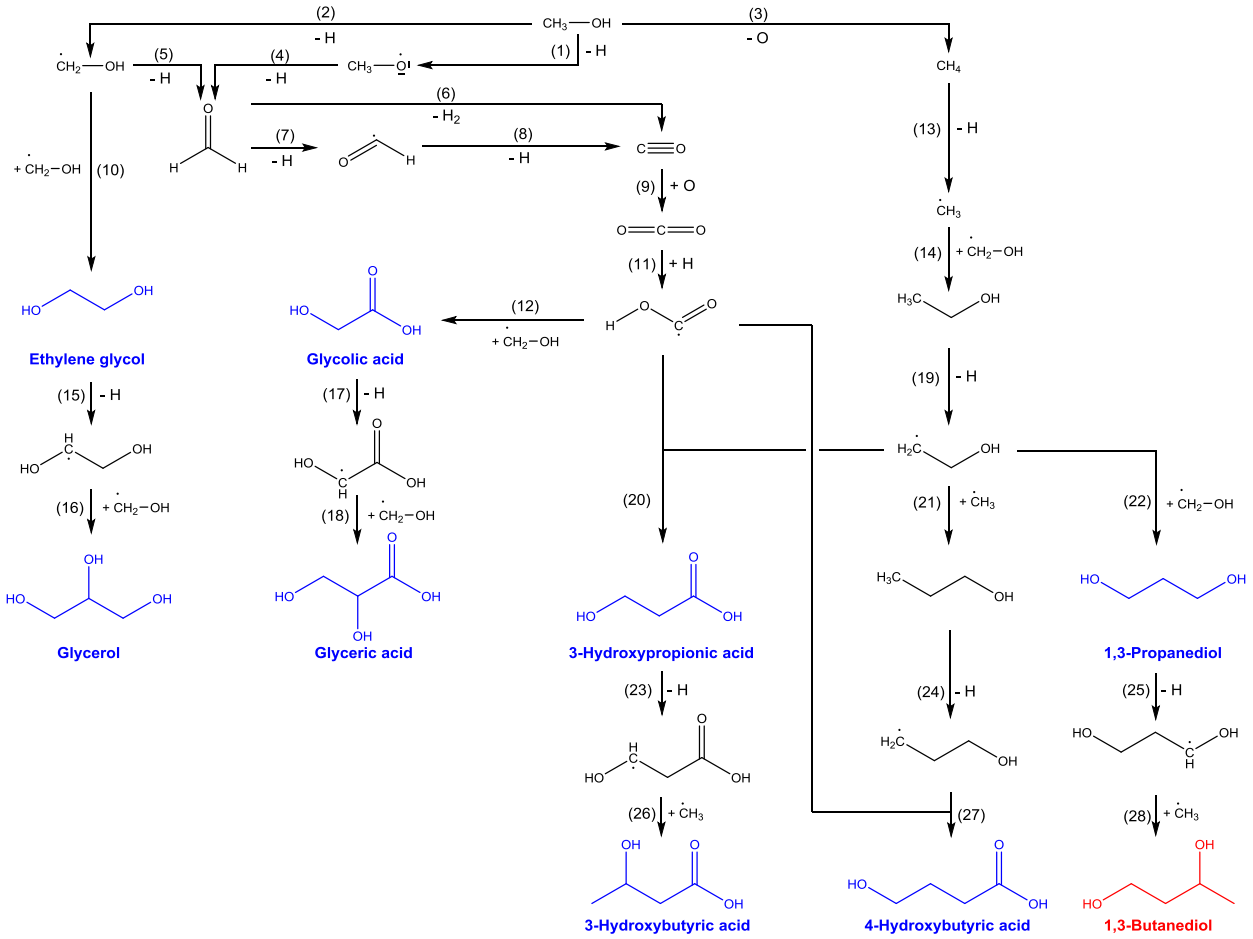

Scheme 1 Proposed formation pathways of the detected polyols and hydroxycarboxylic acids. Species in blue and red are identified in irradiated $CH_3{}^{18}OH$ ices by GC×GC-TOFMS. The one in red has not been reported in previous laboratory studies.

Tables:

Table 1 Compilation of the Identified Polyols and Hydroxycarboxylic Acids ($\leqslant C_4$) in the Interstellar Medium (ISM), Meteorites, and Interstellar Analogous Ices

	Compound	Formula	Reference	
			ISM & Meteorite (1-5)	Interstellar Analog Ices(6-12)
Polyol	Ethylene glycol	$HOCH_2CH_2OH$	(1-3)	(6-8)
	1,3-Propanediol	$HOCH_2CH_2CH_2OH$		(8, 10)
	Glycerol	$HOCH_2CH(OH)CH_2OH$	(3, 4)	(6-9, 11)
	Erythritol & Threitol	$HOCH_2CH(OH)CH(OH)CH_2OH$	(3, 4)	(8)
	2-Methyl glycerol	$HOCH_2C(CH_3)(OH)CH_2OH$		(8)
	2-Hydroxymethyl glycerol	$(HOCH_2)_2C(OH)CH_2OH$	(3)	(8)
Hydroxy-carboxylic acid	Glycolic acid	$HOCH_2COOH$	(5)	(6-9, 12)
	Lactic acid	$CH_3CH(OH)COOH$	(5)	(6-8, 12)
	3-Hydroxypropionic acid	$HOCH_2CH_2COOH$	(5)	(7, 8, 12)
	Glyceric acid	$HOCH_2CH(OH)COOH$	(3, 4)	(6-9, 12)
	2-Hydroxybutyric acid	$CH_3CH_2CH(OH)COOH$	(5)	(8, 12)
	3-Hydroxybutyric acid	$CH_3CH(OH)CH_2COOH$	(5)	(8)
	4-Hydroxybutyric acid	$HOCH_2CH_2CH_2COOH$	(5)	(8)
	2-Hydroxylmethyl glyceric acid	$(HOCH_2)_2C(OH)COOH$	(3)	
	2-Hydroxyisobutyric acid	$(CH_3)_2C(OH)\ COOH$	(5)	(8)
	2, 4-Dihydroxybutyric acid	$HOCH_2CH_2CH(OH)COOH$	(3, 4)	
	2, 3-Dihydroxybutyric acid & diastereomer	$CH_3CH(OH)CH(OH)COOH$	(3, 4)	
	3, 4-Dihydroxybutyric acid	$HOCH_2CH(OH)CH_2COOH$	(3, 4)	
	2-Methyl glyceric acid	$HOCH_2C(CH_3)(OH)COOH$	(3, 4)	(8)
	Erythronic & Threonic acid	$HOCH_2CH(OH)CH(OH)COOH$	(3, 4)	(8)
	3-Hydroxyisobutyric acid	$CH_3CH(CH_2OH)COOH$	(5)	(8)
	Malic acid	$HOOCHCH_2CH(OH)COOH$	(5)	(8)
	Tartaric & Mesotartaric acid	$HOOCHCH(OH)CH(OH)COOH$	(4)	

References.

(1) Hollis et al. (2002), (2) McGuire et al. (2017), (3) Cooper et al. (2016), (4) Cooper and Rios (2001), (5) Monroe and Pizzarello (2011), (6) Agarwal et al. (1985), (7) Briggs et al. (1992), (8) Meinert et al. (2016), (9) Nuevo et al. (2010), (10) Nuevo et al. (2018), (11) Kaiser et al. (2015), (12) Materese et al. (2014).

Table 2 Data Applied to Calculate the Average Irradiation Dose per Molecule

Initial kinetic energy of the electrons, E_{init} (keV)	5
Irradiation current, I (nA)	5000 ± 250
Total number of electrons	$(8.8 \pm 0.9) \times 10^{16}$
Average penetration depth, l (nm)[a]	420 ± 40
Maximum penetration depth, (nm)[a]	675 ± 70
Average kinetic energy of backscattered electrons, E_{bs} (keV)[a]	2.74 ± 0. 27
Fraction of backscattered electrons, f_{bs}[a]	0.15 ± 0.02
Average kinetic energy of transmitted electrons, E_{trans} (keV)[a]	0
Fraction of transmitted electrons, f_{trans}[a]	0
Density of the ice, ρ (g cm^{-3})	1.01 ± 0.03
Irradiated area, A (cm^2)	3.2 ± 0.3
Dose per methanol (eV molecule^{-1})	168.9 ± 26.1

Note.

[a]Parameters obtained from CASINO software v2.42.

Table 3 Absorption Peaks Observed in Pristine CH_3OH and $CH_3{}^{18}OH$ Ices at 10 K[a]

Wavenumber (cm^{-1})		Assignment
CH_3OH	$CH_3{}^{18}OH$	
4396	4396	$\nu_2/\nu_9 + \nu_4/\nu_6/\nu_{10}$
4275	4275	$\nu_2/\nu_9 + \nu_4$
4095	4087	?
4012, 3983, 3954	3981, 3962, 3930	$\nu_2/\nu_9 + \nu_8$
3855	3828	?
3402, 3261, 3048	3386, 3233, 3047	ν_1
2989	2986	ν_2
2963	2960	ν_9
2920	2929	$\nu_4 + \nu_5/\nu_4 + \nu_{10}/\nu_5 + \nu_{10}/2\nu_4/2\nu_{10}/2\nu_5$
2872	2861	$2\nu_5/2\nu_{10}$
2828	2829	ν_3
2820	2813, 2811	$2\nu_6$
2600	2598	$\nu_4 + \nu_{11}/\nu_7 + \nu_4/\nu_6/\nu_{10}$
2525	2522	$\nu_6 + \nu_{11}$
2446	2423	$\nu_6 + \nu_8$
2239	2237	$2\nu_{11}/2\nu_7$
2042	1990	$2\nu_8$
1490	1491	$\nu_8 + \nu_{12}$?
1479	1478	ν_4
1460	1461	ν_{10}
1443	1443	ν_5
1418	1413	ν_6
1161, 1133, 1115	1157, 1132, 1115	ν_7
1049	1037,	ν_{11}
1042, 1024	1020, 1000	ν_8
1003	976	$\nu_8(^{13}C)$
859, 805, 714	832, 718	ν_{12}

Note.

[a]Assignments based on the references Bouilloud et al. (2015) and Maity et al. (2015).

Table 4 New Absorption Peaks Observed in CH_3OH and $CH_3{}^{18}OH$ Ices after the Irradiation at 10 K[a]

Wavenumber (cm^{-1})		Assignment
CH_3OH	$CH_3{}^{18}OH$	
3699	3618	CO_2 ($\nu_1 + \nu_3$)[b]
-	3508	$C^{18}O_2$ ($2\nu_2+\nu_3$)
3410	3401	O–H stretch[b]
3007, 2942,2881, 2733	3008, 2944, 2880, 2740	CH_3, CH_2, and CH stretch (Aliphatic)
2345, 2339	2342	CO_2 (ν_3)
-	2325	$OC^{18}O$ (ν_3)
-	2305, 2304	$C^{18}O_2$ (ν_3)
-	2240	$^{13}C^{18}O_2$ (ν_3)
2276	-	$^{13}CO_2$ (ν_3)
2138, 2136	2137	CO (ν_1)
-	2087	$C^{18}O$ (ν_1)
1844	1802	HCO (ν_3)[b]
1744, 1722, 1708, 1678, 1641	1715, 1686, 1681, 1661, 1622	C=O stretch[b]
1499	1483	H_2CO(ν_3)[b]
1376, 1352, 1330	1378, 1351, 1338	CH bending and OH bending[b]
1304, 1303	1303	CH_4 (ν_4)
1270, 1213, 1199	1273, 1189	CH_2 twisting and OH bending[b]
1089, 1066	1074, 1043, 1014	C–O stretch[b]
917, 895	904, 868	C–C–O stretch[b]
663, 653	653, 344	CO_2 (ν_2)[b]

Notes.

[a]Assignments based on the references Bouilloud et al. (2015), Maity et al. (2015), and Socrates (2004).

[b]For the $CH_3{}^{18}OH$ ice, oxygen atoms are ^{18}O substituted.

Table 5 Absorption Peaks Observed in the Residues of Irradiated CH_3OH and $CH_3{}^{18}OH$ Ices at 300 K[a]

Wavenumber (cm^{-1})		Assignment
CH_3OH	$CH_3{}^{18}OH$	
3449, 3328, 3061	3245, 3051	O–H stretch[b]
2957, 2931, 2885	2964, 2931, 2890	CH_3, CH_2, and CH stretch (Aliphatic)
1721	1691	C=O stretch[b]
1454	1456	CH_2 scissoring
1373, 1325	1375, 1316	CH bending and OH bending[b]
1070, 1031	1058, 1012	C–O stretch[b]

Notes.

[a]Assignments based on the reference Socrates (2004).

[b]For the $CH_3{}^{18}OH$ ice, oxygen atoms are ^{18}O substituted.

Table 6 Identified Compounds as Trimethylsilyl (TMS) Derivatives in Interstellar Analogue Ices Initially Composed of $CH_3{}^{18}OH$ by GC×GC-TOFMS.

Compound	R_{t1}[a] (min)	R_{t2}[b] (s)	MS-fragmentation/^{18}O sample		MS-fragmentation/O reference standard		Relative amount (%)[f]
			$[M^{+\bullet}]$[c]	Other important ions, *m/z*	$[M^{+\bullet}]$[c]	Other important ions, *m/z*	
Ethylene glycol	11.15	1.42	*210*	195, 149, 105, 73	*206*	191, 147, 103, 73	100.00
1,3-Propanediol	13.20	1.41	*224*	209, 181, 149, 132, 117, 73	*220*	205, 177, 147, 130, 115, 73	9.86 ± 0.99
Glycolic acid	13.55	1.78	*226*	211, 181[d], 163, 149, 105, 73	220	205, 177[d], 161, 147, 103, 73	19.58 ± 1.96
1,3-Butanediol[e]	13.60	1.37	*238*	223, 149, 131, 119, 105, 73	234	219, 147, 129, 117, 103, 73	5.21 ± 0.52
3-Hydroxypropionic acid	15.40	1.78	*240*	225, 181[d], 149, 118, 103, 73	234	219, 177[d], 147, 116, 101, 73	13.41 ± 1.34
3-Hydroxybutyric acid	16.05	1.63	*254*	239, 195[d], 149, 119, 73	*248*	233, 191[d], 147, 117, 73	4.83 ± 0.48
4-Hydroxybutyric acid	18.10	1.78	*254*	239, 208[d], 149, 119, 73	*248*	233, 204[d], 147, 117, 73	0.93 ± 0.10
Glycerol	19.10	1.40	*314*	299, 222, 209, 149, 121, 105, 73	*308*	293, 218, 205, 147, 117, 103, 73	14.67 ± 1.47
Glyceric acid	20.35	1.58	*330*	298[d], 209, 193, 179, 149, 121, 73	*322*	292[d], 205, 189, 175, 147, 117, 73	1.85 ± 0.18

Notes.

[a]GC×GC retention time 1st dimension.

[b]GC×GC retention time 2nd dimension.

[c]Molecular ion peak *in italics* not detected.

[d]McLafferty-type (ester migration) rearrangement.

[e]Has not been detected in previous laboratory residues.

[f]Relative amount with respect to ethylene glycol.